EFFECT OF THE LOSS OF SYMMETRY ON THE DISTRIBUTION OF WALL SHEAR STRESSES IN ABDOMINAL AORTIC ANEURYSMS

Anne-Virginie L. B. Salsac
Department of Mechanical and Aerospace Engineering,
University of California, San Diego
La Jolla, California 92037, USA
asalsac@mae.ucsd.edu

Juan C. Lasheras
Department of Mechanical and Aerospace Engineering,
University of California, San Diego
La Jolla, California 92037, USA
lasheras@mae.ucsd.edu

ABSTRACT

Changes in the patterns of mechanical stimuli acting on the walls are thought to play a crucial role in the growth of abdominal aortic aneurysms (AAA). The goal of this study is therefore to measure the wall shear stresses (WSS) and gradients of wall shear stresses (GWSS) in idealized models of AAA under physiologically realistic pulsatile flow conditions. The spatial and temporal distributions of WSS have been derived from the Particle Image Velocimetry measurements of the velocity field inside the aneurysm. Similarly to axisymmetric aneurysms, the flow remains attached to the wall during the systolic acceleration up to very large asymmetry parameters. The geometric asymmetry prevents the formation of a close vortex ring. The non-symmetric vortex that resembles a hairpin engenders a helical flow pattern inside the AAA. The strength of the vortex shed from the proximal anterior wall increases with the asymmetry parameter, until it dominates the flow structure. Alternate patterns of WSS result along the walls, where the endothelial cells are exposed to quasi-steady very low and reversed WSS along the anterior wall and positive higher amplitude WSS along the posterior wall. GWSS are generated around the point of impact of the vortex on the posterior wall and at the aneurysm necks and are also expected to form in the circumferential direction.

INTRODUCTION

An abdominal aortic aneurysm (AAA) is a localized dilatation that forms in the infrarenal abdominal aorta. It is a significant vascular problem, which occurs in 5 to 7 percent of the population over 60 years of age and whose rate of incidence has greatly increased as the population ages (Singh et al., 2001). Age, gender, smoking, hypertension, diabetes, high cholesterol and family history are all known contributing risk factors (Pokrovskii et al., 2003; UK Small Aneurysm Trial, 2000; Reilly and Tilson, 1989). However, the exact causes for the aneurysm formation and expansion are still not understood. A largely accepted hypothesis is that, once an aneurysm forms, it enlarges due to a complex interplay between mechanical stimuli exerted by the pulsatile blood flow on the walls and physiological changes occurring in the wall structure, mainly in the intima and media layers. But, due to the inability of the current imaging devices (CT scans, MRI, ultrasounds, etc.), there has been no successful attempt at measuring the wall shear stresses (WSS) *in vivo* inside a patient's aneurysm with high spatial resolution. A large body of experiments has been conducted experimentally (Fukushima, Matsuzawa and Homma, 1989; Budwig et al., 1993; Egelhoff et al., 1999; Yu and Zhao, 2000; etc.) or numerically (Taylor and Yamaguchi, 1994; Viswanath, Rodkiewicz and Zajac, 1997; Finol and Amon, 2001-2003) in rigid models, looking the hemodynamics inside the AAA, but none of these studies has provided measurements/calculations of the spatial and temporal distribution of the WSS, which is one of the most physiologically relevant parameter. The purpose of this study is therefore to characterize both the distribution of mechanical stimuli acting on the endothelial cells that line the blood vessel. In particular, this study focuses on the effects that the loss of symmetry has on the distribution of WSS and its gradients. This is an important issue from the clinical point of view, since most aneurysms grow in a non-symmetric way due to the presence and support of the spinal column. We have conducted a parametric study, in which the flow characteristics were measured inside fusiform models of AAA, while varying the asymmetry parameter. The hemodynamic stresses acting on the vessel wall are calculated from the quantitative measurements of the velocity field, obtained inside the AAA models using Particle Image Velocimetry (PIV).

MATERIAL AND METHODS

Three aneurysm models have been considered in the study, one symmetric (model 1) and two non-symmetric (models 2 and 3) (see Figure 1). The three models have the same dilatation ratio ($D/d = 2.3$) and aspect ratio ($L/d = 4.5$), but the asymmetry parameter $\beta = 2e/d$ increases from 0 for the symmetric model to 0.5 for model 2 and 1 for model 3. D and L are the maximum internal diameter and the length

of the bulge, d the internal diameter of the parent vessel and e the eccentricity. The eccentricity is defined as the distance between the axis of symmetry of the parent vessel and the centerline at the maximum bulge diameter.

The models are assumed to be devoid of an endoluminal thrombus, which has been observed to typically form when D > 4.5 cm. The choice of an idealized geometry for the models was made in order to control their shape with only three parameters. Although the shape of the models is not physiologically correct, one can hope that all the important physical processes can be observed and measured accurately. The walls are assumed to be rigid, the models being made out of glass. AAAs have been shown to become stiffer as they expand, because of the important degradation of the elastin fibers (Di Martino et al., 1998). In the experiment, it was not necessary to model the actual wall compliance, since the pump reproduces directly the flow waveform measured in the infrarenal abdominal aorta.

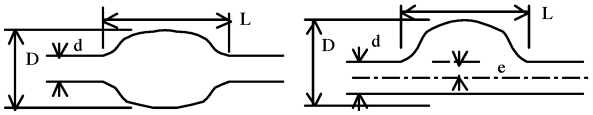

Figure 1: Geometry of the aneurysm models. The side view of the non-symmetric models is shown on the right (for β = 1 in the present case).

The experimental setup is shown in Figure 2. A programmable piston pump reproduces the waveform that Maier et al. (1989) measured in the infrarenal abdominal aortic flow of a healthy male patient at rest (Figure 3). A micro-stepping motor (Compumotor Corporation, Cupertino, CA) controls the displacement of the piston on a rack inside a cylinder. Each time the piston reaches the end of the cylinder, a four-way spool valve (Numatics, Highlands, MI) reverses the inlet and outlet pathways, in order to always keep the flow in the same direction in the test section.

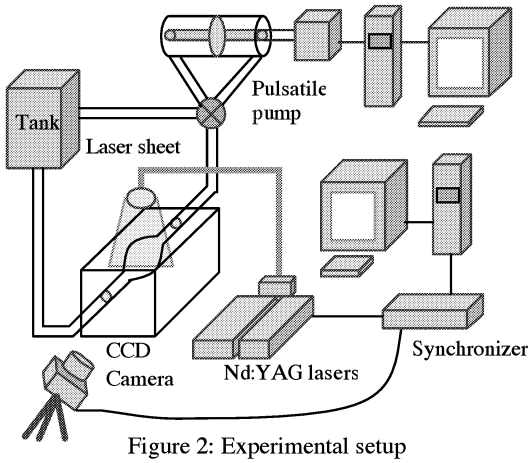

Figure 2: Experimental setup

In order to conduct the Particle Image Velocimetry (PIV) measurements, the system has been perfused with water seeded with 10-μm lycopodium particles (Carolina Biological Supply Company, Burlington, NC). The non-Newtonian behavior of blood has therefore been neglected, which should be a valid assumption in the case of a large blood vessel such as the aorta (d = 1.8 cm) (Nichols and O'Rourke, 1990). Water, which has a viscosity 3.9 times lower than blood, and aneurysm models scaled down by a factor of 1.9 have been used in this experiment in order to remain within the working range of the pulsatile pump. The experiment has been conducted in complete similarity, since both the Reynolds number, $\overline{Re} = \overline{U}d/?$ and the Womersley number, $\alpha = d/2\sqrt{\omega / ?}$, have been kept identical to the physiological flow conditions.

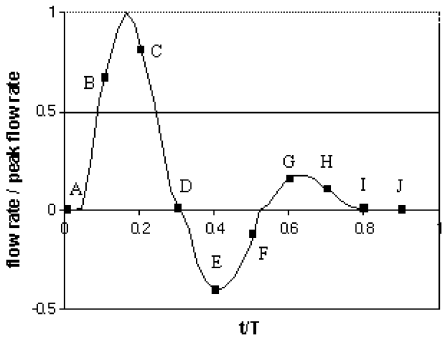

Figure 3: Flow waveform input in the pump, non-dimensionalized by the peak flow rate. The times of measurement are indicated by the letters A, B, etc.

The PIV system (TSI Incorporated, St Paul, MN) is composed of two 50 mJ pulsed Nd:YAG lasers, a synchronizer and a CCD camera (Figure 2). The camera (630046 PIVCAM 10-30) records the positions of the lycopodium particles that are illuminated each time the lasers are fired (10 Hz). The displacements of the particles are obtained by locally cross-correlating pairs of images.

RESULTS

The instantaneous velocity field is shown in Figure 4 inside the symmetric model (model 1) at four representative times along the cardiac cycle. During the systolic acceleration, the flow remains laminar and fully attached to the diverging walls, similarly to the flow in a healthy abdominal aorta. However, the flow detaches from the proximal (upstream) wall in the decelerating phase of the systole (Figure 4 C). The flow separation from the wall is one of the main characteristics of the flow in aneurysms. A strong start-up vortex ring forms proximally and travels along the aneurysm cavity, followed by a free internal shear layer, in which some secondary vortices form (Figure 4 D). The regions of high shear stresses that are typically located at the walls in a healthy vessel are transferred to the bulk of the flow. In the case of the symmetric model, the ratio l/d, where l is the distance available for the vortex ring to travel inside the aneurysm, is equal to 2.5. It is therefore less than the systolic Strouhal number (St_{syst} = 3), which is the controlling parameter of the vortex shedding. The vortex ring therefore impinges on the distal neck of the aneurysm (Figure 4 E), generating very high shear stresses at the point of impact. The impact of the vortex also causes the breakdown of the axisymmetry of the flow and a transition

to a weak turbulence state (Figure 4 F). The intensity of the turbulent structures decreases in the resting period of the cardiac cycle because of viscous dissipation. Some residual structures remain at the end of the cycle, which causes a small cycle-to-cycle variation.

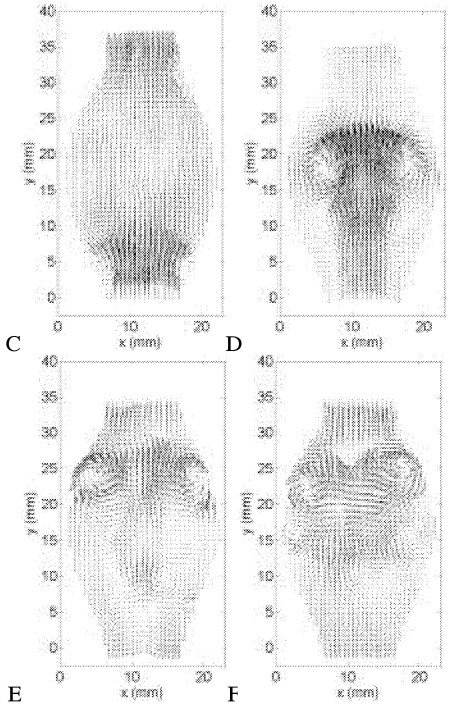

Figure 4: Instantaneous velocity field measured in model 1 with the PIV system

Figure 5 shows the instantaneous velocity field measured with the PIV system in model 2 ($\beta = 0.5$) both in the front and side views of the aneurysm. During the systolic acceleration, no appreciable difference can be observed between the flow in the non-symmetric and symmetric models: the flow remains attached to the walls, since the controlling parameter, the aspect ratio, is identical for all the models (Figure 5 B). But, as the flow decelerates, the flow separates from the side and anterior walls, while staying attached to the posterior wall. This leads to the formation of a hairpin vortex that is not a close vortex ring any longer (Figure 5 C). The vortex moves towards the posterior wall, inducing high shear stresses on the wall at the point of impact (Figure 5 D). Downstream of that point, the flow separates from the wall. In the side view, the vortex persists throughout the cardiac cycle and it is only washed out of the aneurysmal cavity by the systolic push of the following cardiac cycle.

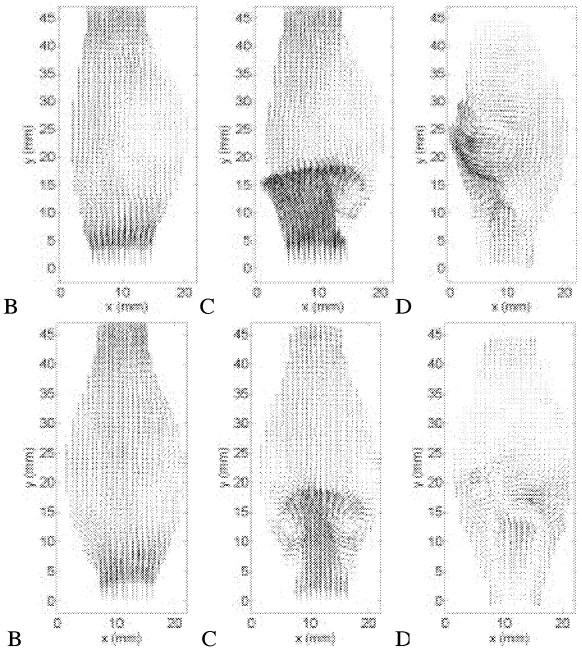

Figure 5: Instantaneous velocity field measured in two perpendicular planes in model 2 ($\beta = 0.5$) with the PIV system

Figure 6 shows the flow field in the non-symmetric plane cut in model 3 ($\beta = 1$), which is characterized by the same dilatation and aspect ratios as model 1, but an asymmetry ratio of 1, corresponding to the most extreme case with a flat posterior wall (Figure 1). One can observed that the flow separation occurs earlier as the asymmetry parameter increases. The increase in the asymmetry parameter also leads to an increase in the strength of the vortex shed from the anterior wall (Figure 6 C). A striking difference with the flow in a symmetric AAA is the formation of a stagnation point along the bulged wall (Figure 6 D). The stagnation point, characterized by a large spike of pressure and gradients of WSS appears towards the point of maximum diameter, damaging the wall at what seems to be its weakest point. In the diastole, the flow is dominated by a weak turbulent state of stronger intensity than in the symmetric case.

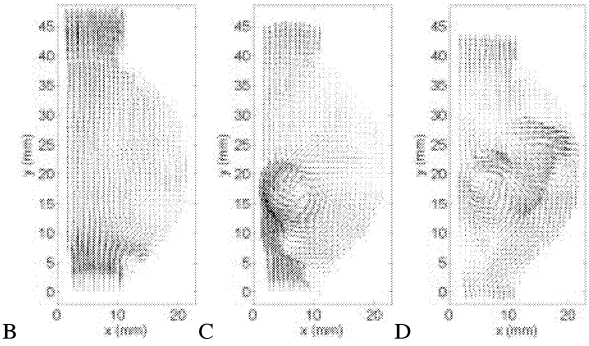

Figure 6: Instantaneous velocity field measured in the side-view plane of model 3 ($\beta = 1$) with the PIV system

The spatial and temporal distributions of wall shear stresses show a decrease in the magnitude of the WSS in the systole in symmetric aneurysms. Since the flow remains attached to the walls during systole, the WSS follows a similar trend to the velocity, which inversely scales with the diameter in order to conserve mass.

Two regions with distinct patterns of WSS and GWSS form inside the aneurysm. The proximal half of the dilatation is dominated by oscillatory WSS of very low magnitude. A single peak in the gradients of WSS is formed at the time of flow detachment. The distal wall, however, is subjected to WSS pointing mainly in the reversed direction and sustained gradients of WSS. This can be seen on the time evolution of the phase-averaged WSS, plotted in Figure 7*a* at two locations (y/L = 0.33 for the proximal half and y/L = 0.71 for the distal half) in the symmetric model (model 1). The WSS profiles are compared with the typical one measured in a healthy abdominal aorta. Figure 8*a* shows the corresponding time evolution of the gradient of the phase-averaged WSS. The measurements in the healthy vessel show that some residual gradients are measured, although the gradients should approach a zero value in this case.

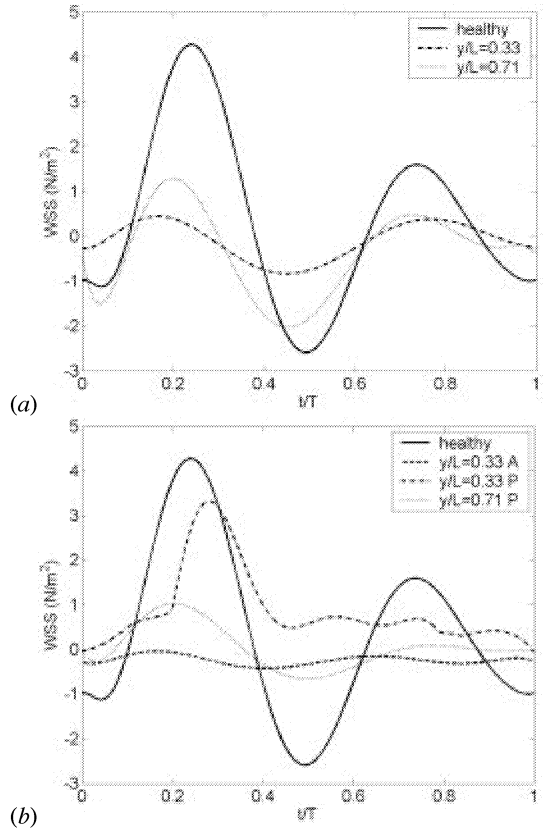

Figure 7: Time evolution of the phase-averaged WSS at a few locations (*a*) in the symmetric model (model 1) and (*b*) in the fully non-symmetric model (model 3, β = 1). A = anterior, P = posterior

In the case of non-symmetric aneurysms, different patterns of stimuli are found along the anterior and posterior walls. With the large region of separated flow along the anterior wall, the wall is subjected to almost inexistent WSS and GWSS. The time evolution of the WSS and GWSS are plotted in Figures 7*b* and 8*b* at one location along the anterior wall (y/L = 0.33) and at two locations along the posterior wall (y/L = 0.33 for the proximal half and y/L = 0.71 for the distal half). One can see that, contrary to the anterior wall, the proximal half of the posterior wall is exposed to larger magnitude, positive shear stresses. However, the shear stresses become oscillatory in the distal part of the wall, where the flow detaches from the wall.

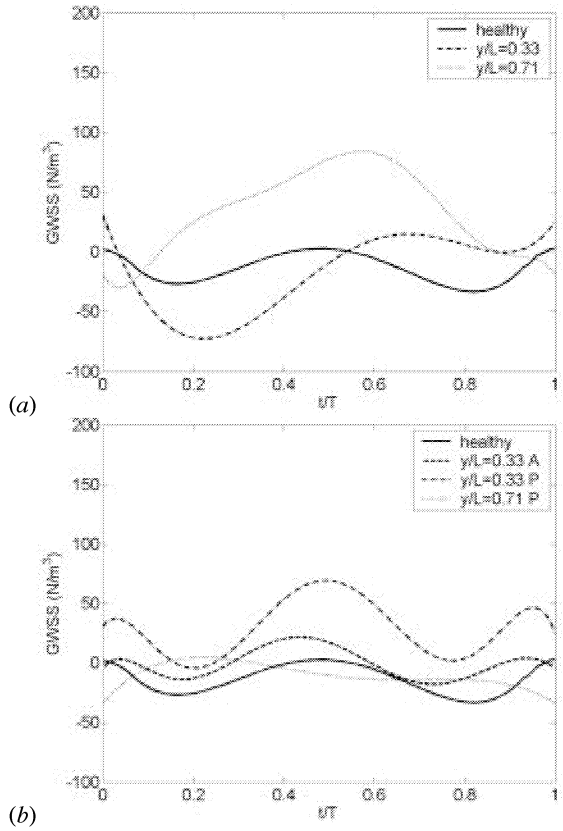

Figure 8: Time evolution of the gradients of the phase-averaged WSS at a few locations (*a*) in the symmetric model (model 1) and (*b*) in the fully non-symmetric model (model 3, β = 1). A = anterior, P = posterior

DISCUSSION

We have measured the spatial and temporal distribution of the wall shear stresses in idealized models of AAA that are characterized by an increasing asymmetry parameter. It has been shown that most of the flow characteristics observed in symmetric aneurysms persist in non-symmetric ones. Up to large asymmetry parameters, the flow remains attached to the walls during the systolic acceleration. This engenders a decrease in the WSS inside the aneurysm as compared to the healthy vessel and therefore large GWSS at both necks. As the asymmetry parameter is increased, the flow detachment occurs earlier in the cardiac cycle. The geometric asymmetry affects flow separation and prevents the formation of a closed vortex ring, since the flow remains attached to the posterior wall. A hairpin vortex forms, the

strongest vortex being shed from the anterior wall, where the wall curvature is maximal. As the vortex progresses inside the cavity, it rotates and becomes elongated, the stretching in the axial direction being more important than in the transverse direction. In the early diastole, the hairpin vortex impinges on the posterior wall.

Associated with this vortex are opposite patterns of WSS for the posterior and anterior walls. Because of the formation of a zone of recirculating flow, the anterior wall is subjected to very low and reversed WSS. Averaged over the length of the aneurysm and one cardiac cycle, the magnitude of the WSS is less than 20% of the value in a healthy aorta. The very low level of stimulation found along the anterior wall is likely to greatly impair the functions of the endothelial cells. At stake is also the uni-directional quasi-steady stress pattern (negative in this case). In a healthy aorta, the endothelium is exposed to pulsatile WSS that become negative only during the diastole. Steady low shear stresses and oscillatory wall shear stresses have been extensively studied in the literature and have been reported to lead to the cell apoptosis (Malek, Alper and Izumo, 1999; Topper et al., 1996; Warabi et al., 2004). In regions of quasi-stasis, the residence times increase drastically, enhancing all the diffusion processes through the walls. The flow conditions found along the anterior wall are therefore likely to promote the accumulation of molecules such as low-density lipoproteins in the intima and media layers, leading to an inflammation of the vessel wall (Caro, Fitz-Gerald, and Schroter, 1971). Platelets and debris are also likely to deposit along the wall. We can thus hypothesize that an endoluminal thrombus may form in these large regions of slowly recirculating flows.

On the opposite wall, the endothelial cells of the proximal half are subjected to only positive WSS (forward flow) of much high amplitude (~60% of healthy value). peak in WSS occurs in the region where the vortex impinges the wall. However, the distal half of the posterior wall experiences oscillating WSS of about 1 N/m^2-amplitude. The variations of the WSS along the wall generated GWSS in the medial section. Furthermore, with the posterior and anterior walls subjected to opposite patterns of WSS, strong circumferential gradients of WSS are likely to be generated.

CONCLUSIONS

It has long been known that the functions of the endothelial cells are sensitive to the local hemodynamic parameters and more specifically to the distribution of shear stresses. Our comparative analysis of the WSS in fusiform models of AAA has shown that, as the asymmetry parameter is increased, the levels of WSS remain in the healthy range on the posterior wall but oscillate around zero on the posterior wall. A spike of WSS is generated on the anterior wall at the stagnation point and very strong gradients of WSS form at the aneurysm necks and upstream and downstream of the strong vortex. The formation of regions of high WSS, low and oscillating WSS, turbulent WSS and high gradients of WSS, which do not exist in a healthy vessel, are likely to strongly contribute to the evolution of the vascular disease processes by triggering various physiological reactions in the arterial wall.

REFERENCES

Budwig, R., Elger, D., Hooper, H., and Slippy, J., 1993, "Steady flow in abdominal aortic aneurysm models," *J. Biomech. Eng.*, Vol. 115, pp. 418-423.

Di Martino, E., Mantero, S., Inzoli, F., Melissano, G., Astore, D., Chiesa, R., and Fumero, R., 1998, "Biomechanics of abdominal aortic aneurysm in the presence of endoluminal thrombus: experimental characterization and structure static computational analysis," *Eur. J. Vasc. Endovasc. Surg.*, Vol. 15, pp. 290-299.

Egelhoff, C. J., Budwig, R. S., Elger, D. F., Khraishi, T. A., and Johansen, K. H., 1999, "Model studies of the flow in abdominal aortic aneurysms during resting and exercise conditions," *J. Biomech.*, Vol. 32, pp. 1319-1329.

Fukushima T., Matsuzawa T., and Homma T., 1989, "Visualization and finite element analysis of pulsatile flow in models of the abdominal aortic aneurysm," *Biorheol.*, Vol. 26, pp. 109-130.

Finol, E. A., and Amon, C. H., 2001, "Blood flow in abdominal aortic aneurysms: pulsatile flow hemodynamics," *J. Biomech. Eng.*, Vol. 123, pp. 474-484.

Finol, E. A., and Amon, C. H., 2003, "Flow dynamics in abdominal aortic aneurysms," *Acta Cient. Venez.*, Vol. 54, pp. 43-49.

Maier, S. E., Meier, D., Boesinger, P., Moser, U. T., Vieli, A., 1989, "Human abdominal aorta: comparative measurements of blood flow with MR imaging and multigated Doppler US," *Radiology*, Vol. 171, pp. 487-492.

Malek, M., Alper, S. L., and Izumo, S., 1999, "Hemodynamic shear stress and its role in atherosclerosis," *JAMA*, Vol. 282, pp. 2035-2042.

Nichols, W. W., and O'Rourke, M. F., 1990, *McDonald's blood flow in arteries: theoretic, experimental and clinical principles*, London, Edward Arnold.

Pokrovskii, A. V., Dan, V. N., Zlatovchen, A. M., and Il'in, S. A., 2003, "The impact of cardiac status and arterial hypertension on the results of surgical treatment of patients over 70 years with abdominal aortic aneurysms," *Angiol. Sosud. Khir.*, Vol. 9, pp. 71-76.

Reilly, J. M., and Tilson, M. D., "Incidence and etiology of abdominal aortic aneurysms," *Surg. Clin. North Am.*, Vol. 69, pp. 705-898.

Singh, K., Bønaa, K. H., Jacobson, B. K., Bjørk, L., and Solberg, S., 2001, "Prevalence of and risk factors for abdominal aortic aneurysms in a population-based study," *Am. J. Epidemiol.*, Vol. 154, pp. 236-244.

Taylor, T. W., and Yamaguchi, T., 1994, "Three-dimensional simulation of blood flow in an abdominal aortic aneurysm – steady and unsteady flow cases," *J. Biomech. Eng.*, Vol. 116, pp. 89-97.

Topper, J. N., Cai, J., Falb, D., and Gimbrone, M A., 1996, "Identification of vascular endothelial genes differentially responsive to fluid mechanical stimuli: cyclooxygenase-2 manganese superoxide dismutase, and endothelial cell nitric oxide synthase are selectively up-regulated by steady laminar shear stress," *Proc. Natl. Acad. Sci. USA.*, Vol. 93, pp. 10417-10422.

UK Small Aneurysm Trial, 2000, "Smoking, lung function and the prognosis of abdominal aortic aneurysm. The UK Small Aneurysm Trial Participants," *Eur. J. Vasc. Endovas. Surg.*, Vol. 19, pp. 636-642.

Viswanath, N., Rodkiewicz, C. M., and Zajac, S., 1997, "On the abdominal aortic aneurysms: pulsatile state considerations," *Med. Eng. Phys*., Vol. 19, pp. 343-351.

Warabi, E., Wada, Y., Kajiwara, H., Kobayashi, M., Koshiba, N., Hisada, T., Shibata, M., Ando, J., Tsuchiya, M., Kodama, T., and Noguchi, N., 2004, "Effect on endothelial cell gene expression of shear stress, oxygen concentration, and low-density lipoprotein as studied by a novel flow cell culture system," *Free Radic. Biol. Med*., Vol. 37, pp. 682-694.

Yu, S. C. M., and Zhao, J. B., 2000, "A particle image velocimetry study on the pulsatile flow characteristics in straight tubes with an asymmetric bulge," *Proc. Inst. Mech. Eng. C*., Vol. 214, pp. 655-671.